NANO LETTERS

pubs.acs.org/NanoLett Letter

Transparent Air Filters with Active Thermal Sterilization

Seonggeun Han,[⊥] Jaewon Kim,[⊥] Youngseok Lee, Junhyuk Bang, Cheol Gyun Kim, Junhwa Choi, Jinki Min, Inho Ha, Yeosang Yoon, Cheol-Heui Yun, Mutya Cruz, Benjamin J. Wiley, and Seung Hwan Ko*

Cite This: https://doi.org/10.1021/acs.nanolett.1c02737 Read Online

ACCESS | Metrics & More | Article Recommendations | Supporting Information

ABSTRACT: The worldwide proliferation of COVID-19 poses the urgent need for sterilizable and transparent air filters to inhibit virus transmission while retaining ease of communication. Here, we introduce copper nanowires to fabricate transparent and self-sterilizable air filters. Copper nanowire air filter (CNAF) allowed visible light penetration, thereby can exhibit facial expressions, helpful for better communication. CNAF effectively captured particulate matter (PM) by mechanical and electrostatic filtration mechanisms. The temperature of CNAF could be controlled by Joule-heating up to 100 °C with thermal stability. CNAF successfully inhibited the growth of *E. coli* because of the oligodynamic effect of copper. With heat sterilization, the antibacterial efficiency against *G. anodireducens* was greatly improved up to 99.3% within 10 min. CNAF showed high reusability with stable filtration efficiency and thermal antibacterial efficacy after five repeated uses. Our result suggests an alternative form of active antimicrobial air filter in preparation for the current and future pandemic situations.

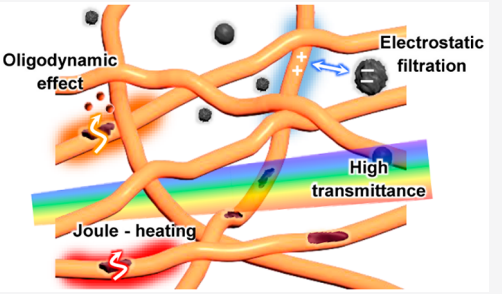

KEYWORDS: *Transparent filter, Air filtration, Copper nanowires, Antimicrobial*

The outbreak of COVID-19 caused by SARS-CoV-2 has extensively impacted the world and devastated every aspect of our life such as health, social relations, economies, and industries.[1−4] Reportedly, COVID-19 spreads through virus-containing particles that are generated when infected people cough, sneeze, talk, and even breathe.[5,6] Those particles exist in the forms of respiratory droplets (>5 μm) or aerosols (≤5 μm) and could be inhaled into the respiratory system of people nearby.[7,8] Consequently, air purification has been recognized as a first step to secure public health from contagious diseases. So far, substantial amounts of air filters have been consumed globally as a key part of air purifying equipment with their remarkable performances in preventing virus transmission and lowering virus infection rate.[9,10]

Still, there remain potential risks about proliferation and secondary transmission of microbes because typical air filters have little antimicrobial ability.[11] Therefore, disinfection of air filters is an emerging topic in the current situation. For this purpose, heat treatment has been widely accepted due to its effective and rapid sterilizing abilities to various microbes while maintaining original filter properties in contrast with organic solvent washing. Additionally, recent studies reported that SARS-CoV and MERS-CoV were rapidly inactivated by heating at 65 °C within 10 min.[12,13] Despite the effectiveness in disinfecting bioaerosols, typical heat treatment necessarily requires separate heating devices, which limits its accessibility in daily life and hinders fast response to real-time sanitization needs. Therefore, efforts have been dedicated to integrating heating functions into air filters mainly by employing photothermal materials.[14,15] However, the light-dependent heating mechanism restricts their usage to the ideal circumstance with sufficient sunlight, not covering other situations such as indoor room, cloudy weather, and nighttime.

Poor transparency is another important issue in the current air filters. This acts as a significant problem especially for current face masks, as they disturb precise communication between people by screening facial expression.[16,17] Considering mandatory wearing of face masks, it might be a huge obstacle to people with hearing loss, who largely depend on such visual information including movements of lips and tongue.[18] Though some researchers have developed transparent nanofiber membranes utilizing novel fabrication methods such as electrospinning and blow spinning, their results did not contain antimicrobial tests.[19−21] Meanwhile, current studies for antimicrobial air filters have paid little attention to optical transparency.[22−24] For these reasons, there exists a demand for a transparent and self-sterilizable air filter.

In this context, copper nanowires (CuNWs) have attractive properties making them a promising solution for realizing these objectives. First, CuNWs could form weblike structures

Received: July 22, 2021
Revised: October 12, 2021

https://doi.org/10.1021/acs.nanolett.1c02737
Nano Lett. XXXX, XXX, XXX−XXX

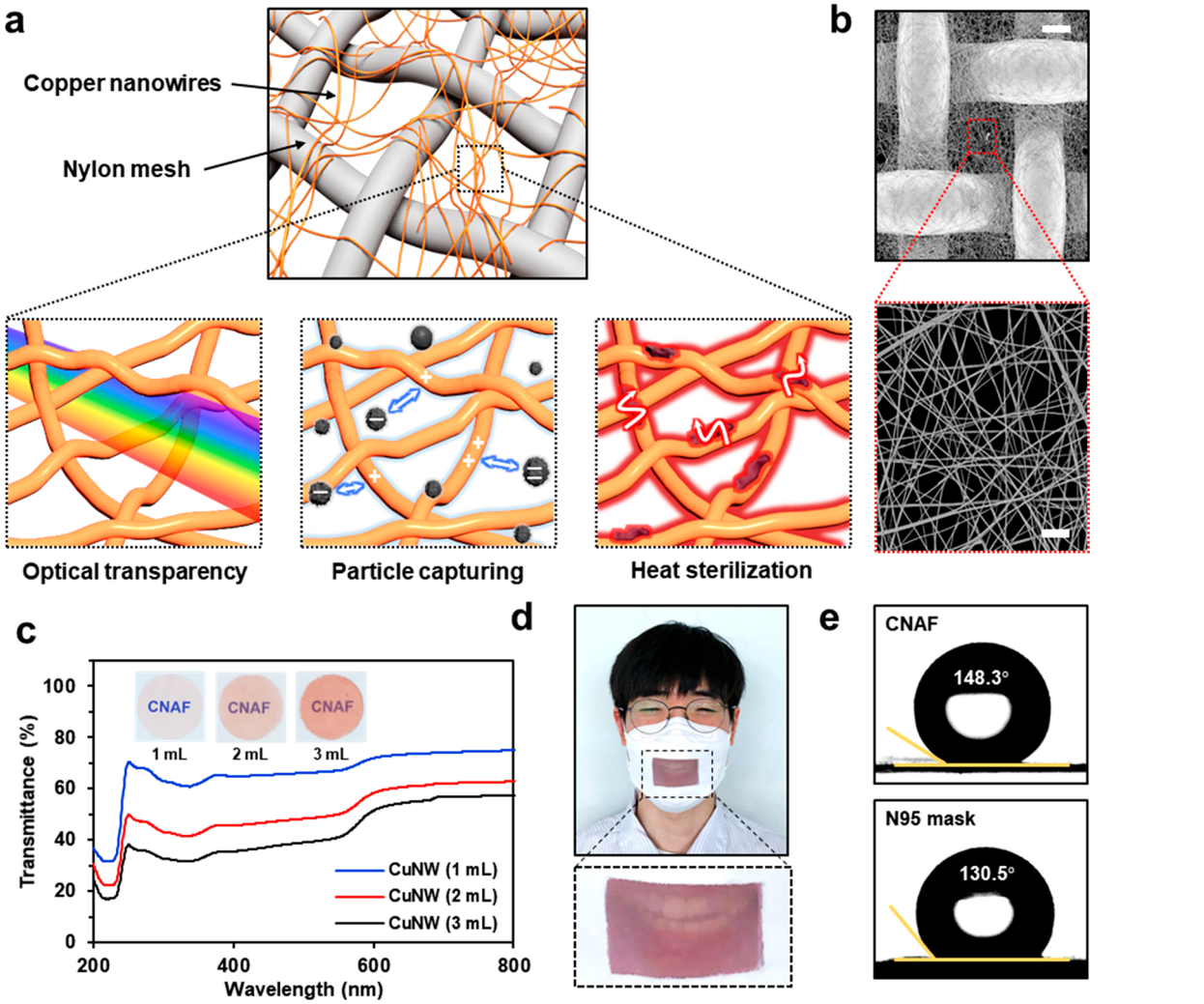

Figure 1. (a) Schematic images of CNAF and its three major capabilities. (b) SEM images of CNAF and CuNW networks on CNAF. The scale bars are 20 and 2 μm, respectively. (c) UV−vis transmittance of CNAF with different amounts of CuNW solution. The insets are corresponding optic images of CNAF. (d) Optic images of a face mask integrated with CNAF. (e) Contact angles of CNAF and N95 mask. Figure 1d courtesy of S. Han.

suitable for capturing bioaerosols. In addition, Cu is an excellent antimicrobial material with its proven sterilization performance, even for SARS-CoV-2.[25−27] Furthermore, CuNW network could be Joule-heated to actively sterilize its surface at various circumstances. Lastly, CuNW network has a high degree of optical transmittance due to the extremely thin nature of CuNWs.

Herein, we prepared copper nanowire air filter (CNAF) and evaluated its bioaerosol protection performances. CNAF can pass visible light with a transmittance up to 70%, enough to exhibit facial expression. For the antimicrobial test, to reduce safety concerns about the lethal virus, two species of bacteria (*Escherichia coli* and *Geobacter anodireducens*) were selected instead as test microbes. CNAF could effectively capture both particulate matter (PM) and aerosolized bacteria. The temperature of CNAF can be elevated up to 100 °C with high thermal stability. By chemical disinfection mechanism, CNAF effectively deactivated captured *E. coli*, which could not be achieved by a commercial mask. Furthermore, antibacterial efficacy for metal-resistant *G. anodireducens* was considerably enhanced to 99.3% under heat treatment. CNAF showed negligible degradation of antibacterial and filtration performances after five times of repeated tests. We further demonstrated its potential application as a transparent and self-sterilizable face mask.

RESULTS AND DISCUSSION

Figure 1a schematically illustrates as-fabricated CNAF with its featured functionalities; (i) light transparency through CuNW network, (ii) particle capturing by mechanical and electrostatic filtration, and (iii) heat sterilization combined with the antibacterial ability of Cu. To fabricate CNAF, CuNWs with a length of ∼100 μm (Figure S1) were synthesized by the hydrothermal method as previously reported.[28] After purified by successive centrifugation and cleaning, CuNWs were deposited onto nylon mesh through the vacuum filtration process. Because the length of CuNWs is longer than an opening of nylon mesh (48 μm), CuNWs could form a weblike structure without penetrating through mesh pores. The CuNW network on the opening region of the nylon mesh, resembling fibrous structures of nonwoven membranes, was verified by scanning electron microscope (SEM) (Figure 1b). Numerous CuNWs are heavily intertwined and construct narrow pores with a size of ∼2 μm, capable of mechanically and electrically

https://doi.org/10.1021/acs.nanolett.1c02737
Nano Lett. XXXX, XXX, XXX−XXX

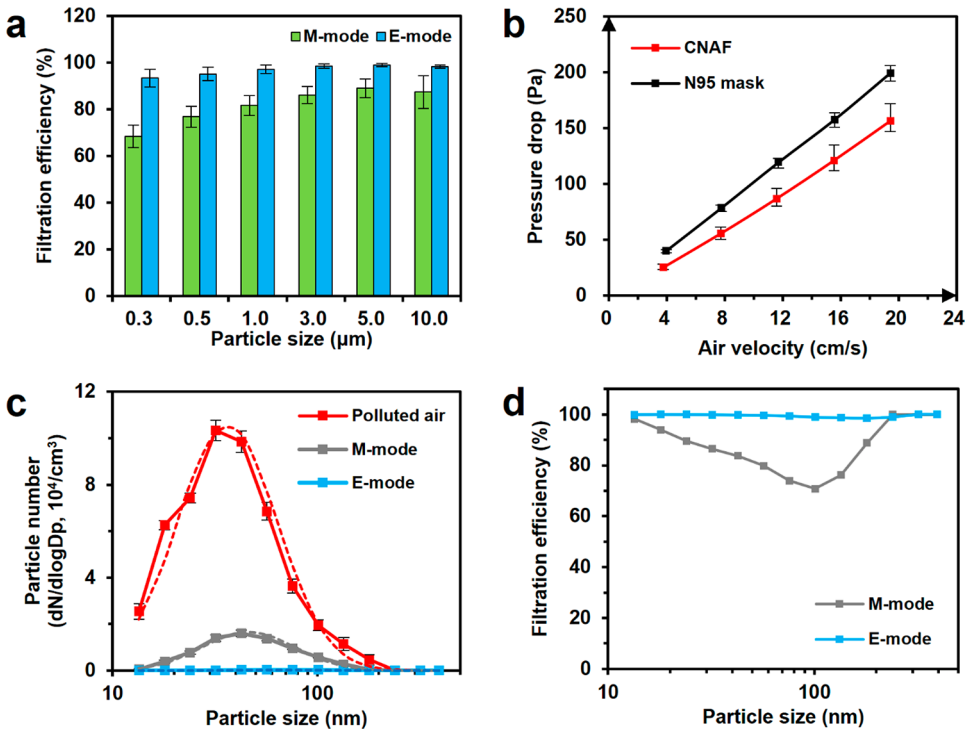

Figure 2. (a) PM capturing efficiency of M-mode and E-mode CNAF for different particle sizes. (b) Pressure drop of CNAF and N95 mask under different air velocities. (c) Particle concentration at nanoranges before and after filtration with M-mode and E mode operated, respectively. Dash lines are trend lines of each. (d) Filtration efficiencies of CNAF under M-mode and E-mode, respectively, for nanosized particles.

capturing PM. Smaller pore and denser networks were observed with increasing amounts of CuNW solution (Figure S2).

As their typical applications to transparent electronics, CuNWs could impart transparency to the air filter.[28,29] Figure 1c presents transmittances of CNAFs, measured by ultraviolet−visible (UV−vis) spectroscopy. Varying the amounts of CuNW solutions, moderate transmittances up to 70% were achieved within the visible wavelength region. To further demonstrate their application as a transparent face mask, CNAF was integrated with the commercial face mask (Supporting Information and Materials and Methods). While wearing the mask, facial expressions were clearly seen through the CNAF (Figure 1d), which is expected to enhance the accuracy of communications.[30,31]

One important aspect of air filter to be considered is surface protection from hazardous biomaterials.[32,33] Because many respiratory diseases, including COVID-19, spread through droplets carrying infectious microbes, the hydrophobic surface is beneficial to maintaining a clean surface by repelling the droplets.[7] Contact angles of the water droplet on CNAF and the N95 mask were measured to evaluate their nonwetting abilities (Figure 1e). CNAF showed enhanced hydrophobicity with a contact angle of 148.3° compared to the N95 mask (130.5°). Seemingly, it could be attributed to hydrophobic Cu_2O layer formed on CuNWs during post thermal annealing process.[34]

Overall filtration performances of CNAF were evaluated by a custom-built test setup (Figure S3). Basically, CNAF operates in mechanical filtration mode (M-mode), which is dependent on mechanical capturing mechanisms such as Brownian diffusion, interception, and impaction.[35,36] CNAF also functions in electrostatic filtration mode (E-mode) with the additional engagement of Coulomb force between its surface and aerosols.[36] For this purpose, the negative carbon fiber ionizer was installed in front of electrically grounded CNAF. Because CuNWs were electrically conductive, an electric field was induced on CNAF, and thereby it was able to electrostatically collect the negatively charged aerosols.

Figure 2a presents filtration efficiencies of CNAF for particles with sizes of 0.3, 0.5, 1.0, 3.0, 5.0, and 10.0 μm. Operated at M-mode, CNAF showed filtration efficiencies of 68.4%, 76.8%, 81.6%, 86.1%, 89.0%, and 87.4% for particles from PM0.3 to PM10.0. Considering typical droplet transmission (>5 μm), M-mode CNAF is expected to be effective in inhibiting penetration of those infectious particles. With E-mode operation, filtration efficiencies were greatly enhanced to 93.4%, 95.1%, 97.1%, 98.6%, 99.0%, and 98.2% for the same particle distribution. The enhancement was greater for submicrometer particles owing to electrostatic attraction, stronger and broader than van der Waals force.[35] To compare the filtering characteristics of both modes, PM capturing tests were conducted for severely polluted air generated from burning incense. E-mode CNAF captured more PM than M-mode CNAF at the same time with additional involvement of the mesh region electrostatically attracting PM (Figure S4). Figure 2b illustrates the pressure drop of CNAF and N95 mask according to airflows. For both cases, pressure drop linearly increased with air velocity from 4 to 20 cm/s. Notably, CNAF exhibited lower pressure drop within the overall airflow range, indicating better breathability than commercialized air filters. CNAF was further tested with an automated filter tester, which showed consistent filtration performance (Table S1).

Although there is controversy about an aerosol-mediated virus infection, some researchers have shown evidence for aerosol transmissions.[7,37] Accordingly, filtration efficiencies of CNAF on ultrafine particles (UFPs) were evaluated. Figure 2c shows nanoparticle distributions before and after filtration,

https://doi.org/10.1021/acs.nanolett.1c02737
Nano Lett. XXXX, XXX, XXX−XXX

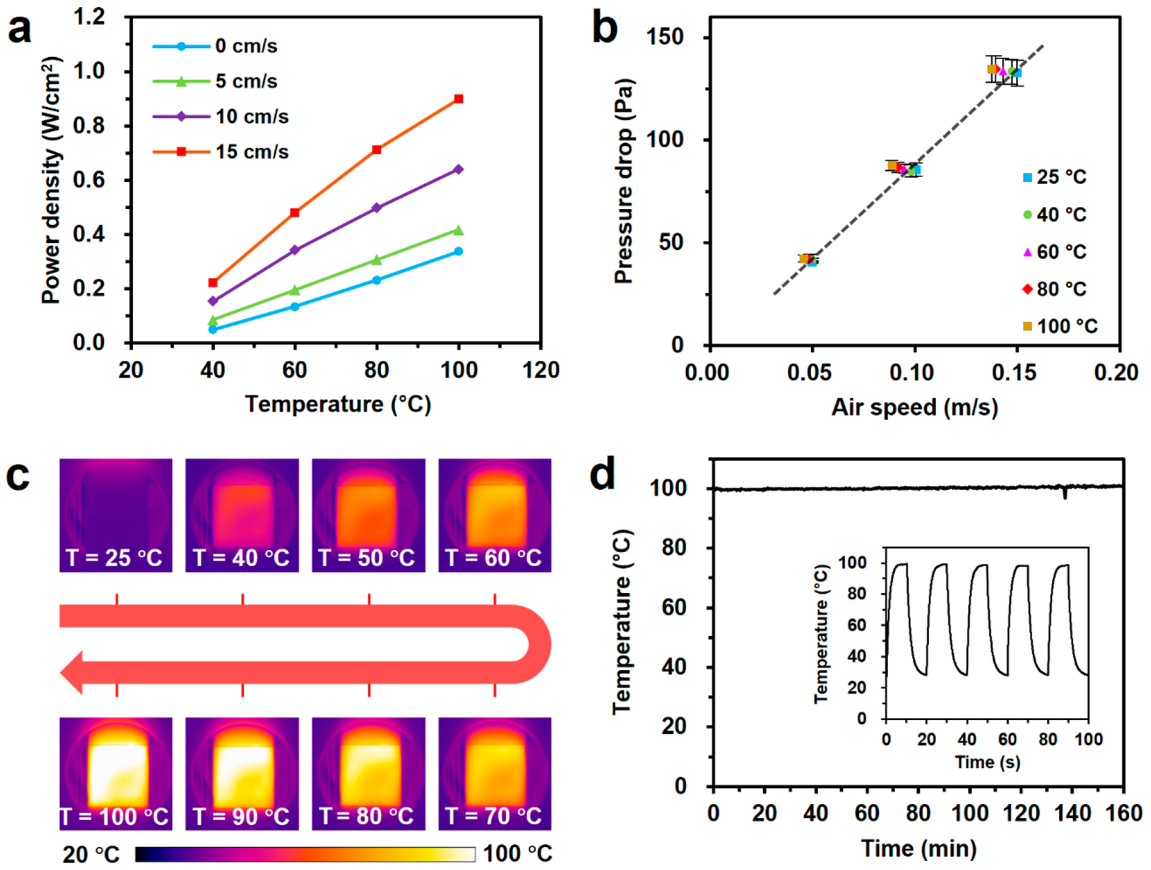

Figure 3. (a) Power consumption of Joule-heating CNAF at different temperatures with regard to different airflows. (b) Pressure drop across CNAF for different airflows at each heating temperature. (c) IR images of CNAF at each heating temperature. (d) Highest temperature under cyclic on−off Joule-heating at the target temperature of 100 °C of CNAF. The inset graph is the temperature of CNAF at the first 5 cycles.

measured by a scanning mobility particle sizer. Polluted air had substantial amounts of nanoparticles peaked at ∼30 nm with over $10^5/cm^3$ concentration. After M-mode, the maximum nanoparticle distribution decreased to 15 900/cm^3. With E-mode, extremely low concentration was observed throughout all size ranges. Compared to M-mode, showing low filtration efficiency around ∼100 nm, E-mode had remarkably high efficiency for all particle sizes (Figure 2d).

Additional experiments were conducted to verify whether nanowires are released from CNAF during its operation (Figure S5). First, the amount of CuNWs detached from CNAF was directly evaluated by a particle sizer (TSI 3910) referring to the previous study.[24] Second, CNAF and nylon membrane stacked in series were suctioned by vacuum pump so that all of the particles released from the former one could be collected by the latter one, and then the chemical composition of nylon membrane was analyzed through energy dispersive spectroscopy (EDS). Lastly, we measured the electrical resistance of CNAF under airflows in real-time to verify whether it increased due to the delamination of CuNWs. For all experiments, we could not observe noticeable evidence of released CuNWs (Figure S5).

Contrary to the conventional air filter made of non-conducting polymeric fibers, CNAF could be thermally sterilized through Joule-heating by allowing electric current. Under airflows, the temperature of CNAF could be controlled by adjusting input power, enabling simultaneous air filtration and sterilization. Figure 3a shows the relation between electric power and the temperature of CNAF for airspeeds from 0 to 15 cm/s. For all conditions, the temperature linearly increased with power consumption. Under the ambient circumstance, CNAF could be heated up to 100 °C with a power density of 0.34 W/cm^2. For higher airspeed, more power was needed to compensate for heat dissipation by air convection. CNAF showed a nearly constant temperature coefficient of resistance under different air flows and could thereby monitor and adjust the temperature itself (Figure S6).

Structural deformation due to heat should be also considered because air permeability is highly dependent on filter geometry. Some materials with a negative coefficient of thermal expansion (CTE) could increase the pressure drop across air filters under elevated temperatures.[38,39] Oppositely, materials with positive CTE might deteriorate filtration efficiency by broadening pore size. To examine the air permeability variance of CNAF under heat treatment, we plotted the relationship between pressure drop and airspeed at elevated surface temperature (Figure 3b). CNAF barely exhibited changes in flow characteristics, indicating it could maintain its original filtration performance cooperating with Joule-heating. Figure 3c presents infrared (IR) images of CNAF, showing that the surface area was evenly heated at different temperatures.

To further confirm the thermal stability of CNAF, 500 cycles of heating and cooling were conducted with the target temperature of 100 °C. The maximum temperature was maintained during the whole cycle, demonstrating stable heating behavior for long-term usage (Figure 3d). Further, CNAF was rapidly heated and cooled within 5 s, attributed to

https://doi.org/10.1021/acs.nanolett.1c02737
Nano Lett. XXXX, XXX, XXX−XXX

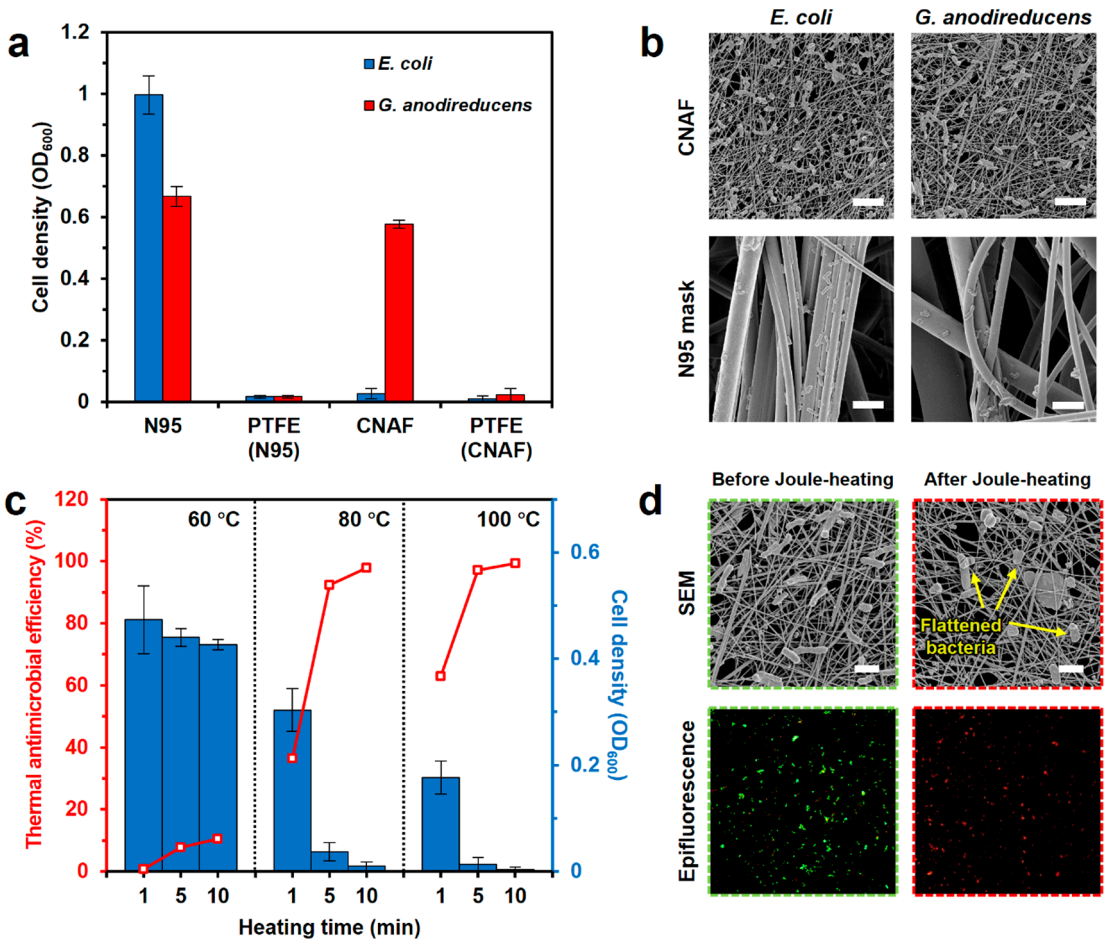

Figure 4. (a) Growth of *E. coli* and *G. anodireducens* on CNAF, N95 mask, and corresponding backing PTFE membrane filter. (b) SEM images of CNAF and N95 mask capturing *E. coli* and *G. anodireducens*. The scale bars are 5 μm. (c) Bacterial growth and corresponding thermal antimicrobial efficiencies of CNAF at different temperatures for different heating times. (d) SEM and epifluorescence images of thermally treated (at 100 °C for 5 min) and untreated *G. anodireducens* on CNAF.

CuNW networks having low heat capacity and large surface area. This rapid temperature response can help to save energy consumption under Joule-heating operation.

As an example of a self-sterilizable air-purifying application, CNAF was integrated into a face mask with a support frame. Keeping appropriate gaps from the face by the support frame, the mask could be effectively heated up to 80 °C without skin damage (Figure S7). Further, considering safety concerns about skin burn by instant contact with CNAF, we modeled the heat transfer process between CNAF and the human skin for the accidental touch (Supporting Information Note 1).[40−42] Additionally, the surface temperature of CNAF attached to the hand was monitored. As a result, short-term touch with heated CNAF did not cause abrupt elevation of skin temperature over 43 °C, where thermal damage is observed,[43] and therefore resulting skin burn might not be expected (Figure S9).

CNAF can function as an antimicrobial filter with two unique characteristics: the oligodynamic effect of Cu and the Joule-heating of CuNW network. The oligodynamic effect is an antibacterial behavior of metal ions, absorbed by bacteria in contact and damaging its cell membrane.[44,45] Heat could induce various antimicrobial effects, including ribonucleic acid (RNA) breakdown and protein denaturation.[46,47] To examine the oligodynamic and Joule-heating effects of CNAF, *E. coli* and *G. anodireducens* were selected, respectively. *E. coli* have been broadly utilized for demonstrating the sterilizing effect and are known to be inactivated by Cu.[48,49] On the contrary, *G. anodireducens* can act as an electron transport medium for microbial fuel cells and are verified to form biofilms on copper, demonstrating the growth of *G. anodireducens* are undisturbed by the oligodynamic effect of Cu, thus the sole antibacterial effect of Joule-heating can be verified.[50−52]

Antibacterial behaviors were analyzed using a bacterial test setup, and a detailed description of the test is shown in Figure S10. Aerosolized bacteria were first filtered by test filters (CNAF and N95 mask), and then all the remaining bacteria were collected by PTFE membranes behind test filters. After each filter was cultured as described in Supporting Information Materials and Methods, optical density at 600 nm (OD_{600}) was measured. Bacterial growth for all PTFE filters was hardly observed, indicating CNAF and N95 mask sufficiently filtered out bacteria (Figure 4a). It has to be noted that *E. coil* on CNAF barely grew, whereas those on the N95 mask showed prominent growth, ascribed to the outstanding antibacterial effect of Cu. Meanwhile, *G. anodireducens* on CNAF were cultured up to a similar level to those on N95 mask, indicating they are oligodynamic effect-resistant as expected. Figure 4b shows SEM images of bacteria seized on CNAF and N95 mask, which reconfirmed the capturing performance of CNAF.

To scrutinize the antibacterial effect of thermal treatment, CNAF capturing *G. anodireducens* was Joule-heated at 60, 80,

https://doi.org/10.1021/acs.nanolett.1c02737
Nano Lett. XXXX, XXX, XXX−XXX

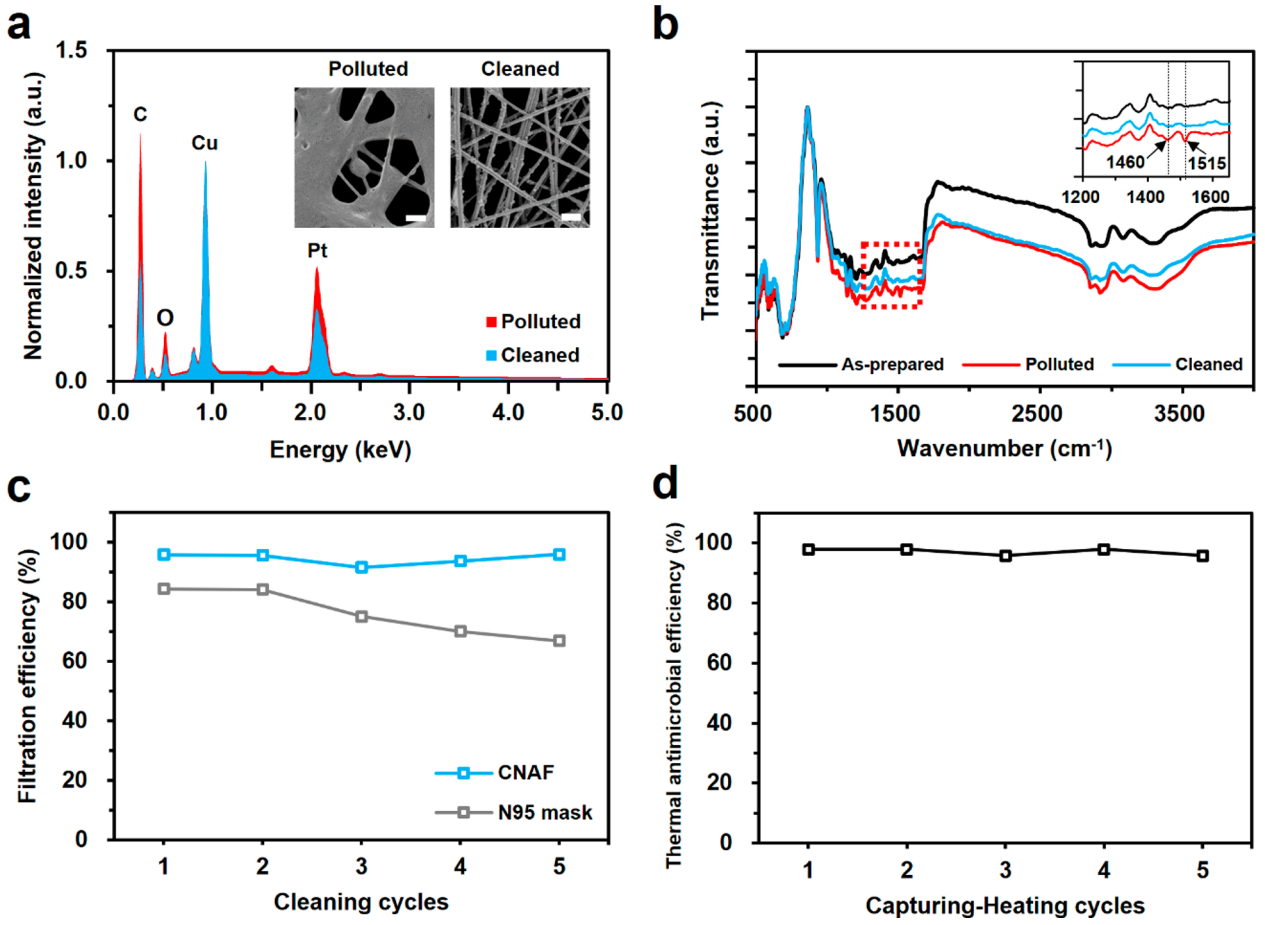

Figure 5. (a) EDS spectrum of CNAF polluted with PM and cleaned by EG/ethanol solutions, respectively. The insets are their SEM images. The scale bars in the insets are 400 nm. (b) FT-IR transmittance of as-prepared, polluted, and cleaned CNAF. The inset is FT-IR transmittance of a shorter wavenumber range. (c) Filtration cycle test with cleaning processes for CNAF and N95 mask for PM with 0.3−10 μm size. (d) Thermal antimicrobial cycle test for *G. anodireducens* of CNAF with heat treatment at 100 °C for 5 min.

and 100 °C for 1, 5, and 10 min, respectively, and then CNAF samples were incubated at 37 °C for 48 h. Heat treatment at 60 °C for 10 min showed an only slight antibacterial effect (10.5%), whereas heat treatment at 80 and 100 °C for 10 min achieved outstanding antimicrobial efficiency of 97.9% and 99.3%, respectively, proving fully sterilized CNAF can be assured via Joule-heating (Figure 4c). Notably, 1 min thermal impact at 80 and 100 °C demonstrated a highly enhanced bacterial killing effect of 36.4% and 62.9%, respectively, compared to heat treatment at 60 °C. Considering this short time scale of Joule-heating, active sterilization can be implemented along with the urgent demand for disinfection, where potential health risks such as pathogens and viruses are likely to exist.

Figure 4d displays SEM and epifluorescence microscopy images of thermally untreated and treated *G. anodireducens* collected on CNAF. The morphology of heat-treated bacteria was flattened, showing inactivation effects of Joule-heating. Likewise, live/dead cell staining displays that dead cells (in red) are dominant, whereas live cells (in green) are almost invisible with heat treatment at 100 °C for 5 min, indicating most *G. anodireducens* were inactivated by thermal treatment.[15] Furthermore, PBS solutions that are containing *E. coli* from pristine CNAF and *G. anodireducens* from heat-treated CNAF, respectively, were inoculated on the agar plates. Both samples showed a low number of colony-forming units (CFU), reconfirming the high antibacterial activity of CNAF (Figure S11).

Since heedless use of disposable air filters can cause severe environmental issues, reusability is a highly required property for air filters.[53] To prove the high renewability, CNAF was severely polluted on purpose and washed by ethanol and ethylene glycol (EG)/ethanol solutions, respectively. For EG/ethanol solution cleaning, most of PM was washed out due to the high dipole moment of EG while a pristine morphology of CNAF was retained. On the other hand, considerable PM remained on CNAF cleaned by ethanol (Figure S12).[54] EDS spectrum of cleaned CNAF indicates that C peak (0.28 keV) and O peak (0.53 keV) were greatly lowered, compared to those of polluted CNAF, demonstrating the removal of PM (Figure 5a).[55] Figure 5b represents FT-IR measurement of as-prepared, polluted, and cleaned CNAF. It is noted that peaks of C−H bond bending (~1460 cm^{-1}) and N−O bond stretching (~1510 cm^{-1}) were reduced after the cleaning process.[56,57] Furthermore, UV−vis transmittance of cleaned CNAF was similar to that of pristine one, consistent with previous characterizations (Figure S13).[54]

We performed a cyclic filtration test for CNAF and N95 mask with a cleaning process conducted after each cycle. Figure 5c reveals that E-mode CNAF preserved high filtration efficiency of 95.9% at the fifth cycle, compared to the N95 mask showing a rapid decrease of filtration efficiency along

https://doi.org/10.1021/acs.nanolett.1c02737
Nano Lett. XXXX, XXX, XXX−XXX

with washing cycles. Further, we conducted a cyclic Joule-heat sterilization test, where aerosolized *G. anodireducens* were filtered for 30 min and heat-treated at 100 °C for 5 min for each cycle. Despite the accumulation of bacteria on CNAF as cycles were repeated, it demonstrated high thermal-killing efficiency of 95.8% at the fifth cycles (Figure 5d). Therefore, CNAF can enhance long-term usability with high filtration efficiency and thermal sterilization ability.

CONCLUSION

In this study, we introduced a transparent copper nanowire air filter, capable of airborne particle capturing and bacterial sterilizing, meriting from the percolated conductive nanowire network and antibacterial copper. Particulate matter and bacteria can be effectively filtered by narrow-sized pores of CNAF. Filtration performance for submicrometer particles was greatly enhanced up to 93.4% by an electrostatic filtration mechanism with a lower pressure drop than a commercial N95 mask. The oligodynamic effect of CuNWs effectively suppressed the growth of *E. coli* on CNAF, compared to that on the N95 mask. Moreover, antibacterial efficiency for *G. anodireducens* was greatly enhanced up to 99.3% within 10 min at 100 °C with the assistance of Joule-heating. CNAF can be reutilized by a facile cleaning process retaining a high filtration efficiency of 95.9% at the fifth cycle. CNAF also maintained high thermal antibacterial performance for five cycles, proving active sterilization can be steadily carried out. We demonstrated CNAF integrated face mask with high transparency and stable Joule-heating operation. Besides, we expect that the fabrication of CNAF could be more scalable through similar kinds of solution-based processes such as roll-to-roll (R2R) and slot-die coating. We trust that this multifunctional CNAF could be a powerful tool for a worldwide peril provoked by PM and contagious microbial, maintaining social connectedness.

ASSOCIATED CONTENT

Supporting Information

The Supporting Information is available free of charge at https://pubs.acs.org/doi/10.1021/acs.nanolett.1c02737.

SEM images of synthesized CuNWs; SEM images of CNAF; schematic image of an experimental setup for filtration performance test; SEM images of CNAF filtering PM; schematic images of measuring released CuNW setup, the comparison of particle concentrations, EDS spectrum of the backing nylon membrane, and resistance variance of CNAF with air flows; normalized resistance of CNAF under heat treatment; optic and IR images of a face mask integrated with CNAF; illustrations of instant contact of CNAF with skin and cross-section of the skin; graph of skin surface temperatures; an optic image of the bacterial capture test setup and schematic diagrams of the bacterial test; inoculations of bacteria on agar plates; SEM images of CNAF before and after cleaning process; UV−vis transmittance of as-prepared, polluted, and cleaned CNAF; durability test of CNAF; physical properties of the human skin; filtering performance of CNAF under standard conditions (PDF)

AUTHOR INFORMATION

Corresponding Author

Seung Hwan Ko − *Applied Nano and Thermal Science Lab, Department of Mechanical Engineering, Seoul National University, Gwanak-gu, Seoul 08826, Republic of Korea; Institute of Advanced Machines and Design/Institute of Engineering Research, Seoul National University, Gwanak-gu, Seoul 08826, Korea;* orcid.org/0000-0002-7477-0820; Email: maxko@snu.ac.kr

Authors

Seonggeun Han − *Applied Nano and Thermal Science Lab, Department of Mechanical Engineering, Seoul National University, Gwanak-gu, Seoul 08826, Republic of Korea*

Jaewon Kim − *Applied Nano and Thermal Science Lab, Department of Mechanical Engineering, Seoul National University, Gwanak-gu, Seoul 08826, Republic of Korea*

Youngseok Lee − *Applied Nano and Thermal Science Lab, Department of Mechanical Engineering, Seoul National University, Gwanak-gu, Seoul 08826, Republic of Korea*

Junhyuk Bang − *Applied Nano and Thermal Science Lab, Department of Mechanical Engineering, Seoul National University, Gwanak-gu, Seoul 08826, Republic of Korea*

Cheol Gyun Kim − *Department of Agricultural Biotechnology, and Research Institute of Agriculture and Life Sciences, Seoul National University, Gwanak-gu, Seoul 08826, Republic of Korea*

Junhwa Choi − *Applied Nano and Thermal Science Lab, Department of Mechanical Engineering, Seoul National University, Gwanak-gu, Seoul 08826, Republic of Korea*

Jinki Min − *Applied Nano and Thermal Science Lab, Department of Mechanical Engineering, Seoul National University, Gwanak-gu, Seoul 08826, Republic of Korea*

Inho Ha − *Applied Nano and Thermal Science Lab, Department of Mechanical Engineering, Seoul National University, Gwanak-gu, Seoul 08826, Republic of Korea*

Yeosang Yoon − *Applied Nano and Thermal Science Lab, Department of Mechanical Engineering, Seoul National University, Gwanak-gu, Seoul 08826, Republic of Korea*

Cheol-Heui Yun − *Department of Agricultural Biotechnology, and Research Institute of Agriculture and Life Sciences, Seoul National University, Gwanak-gu, Seoul 08826, Republic of Korea*

Mutya Cruz − *Department of Chemistry, Duke University, Durham, North Carolina 27708, United States*

Benjamin J. Wiley − *Department of Chemistry, Duke University, Durham, North Carolina 27708, United States*

Complete contact information is available at: https://pubs.acs.org/10.1021/acs.nanolett.1c02737

Author Contributions

⊥S.H. and J.K. contributed equally to this work.

Notes

The authors declare no competing financial interest.

ACKNOWLEDGMENTS

This work is supported by the National Research Foundation of Korea (NRF) Grant (NRF-2021R1A2B5B03001691, 2016R1A5A1938472). We thank Professor Jooyoun Kim for granting access to the automated filter tester. We acknowledge the valuable advice from Kyun Kyu Kim, Seongmin Jeong, and Seojin Jung.

https://doi.org/10.1021/acs.nanolett.1c02737
Nano Lett. XXXX, XXX, XXX−XXX

REFERENCES

(1) Peeri, N. C.; Shrestha, N.; Rahman, M. S.; Zaki, R.; Tan, Z.; Bibi, S.; Baghbanzadeh, M.; Aghamohammadi, N.; Zhang, W.; Haque, U. The SARS, MERS and novel coronavirus (COVID-19) epidemics, the newest and biggest global health threats: what lessons have we learned? *International journal of epidemiology* **2020**, *49* (3), 717−726.

(2) Ozili, P. K.; Arun, T. Spillover of COVID-19: impact on the Global Economy. *SSRN* **2020**, DOI: DOI: 10.2139/ssrn.3562570 (accessed 2021-05-11).

(3) Dube, K.; Nhamo, G.; Chikodzi, D. COVID-19 cripples global restaurant and hospitality industry. *Current Issues in Tourism* **2021**, *24* (11), 1487−1490.

(4) Chakraborty, I.; Maity, P. COVID-19 outbreak: Migration, effects on society, global environment and prevention. *Sci. Total Environ.* **2020**, *728*, 138882.

(5) Lai, C.-C.; Shih, T.-P.; Ko, W.-C.; Tang, H.-J.; Hsueh, P.-R. Severe acute respiratory syndrome coronavirus 2 (SARS-CoV-2) and coronavirus disease-2019 (COVID-19): The epidemic and the challenges. *Int. J. Antimicrob. Agents* **2020**, *55* (3), 105924.

(6) Santarpia, J. L.; Rivera, D. N.; Herrera, V. L.; Morwitzer, M. J.; Creager, H. M.; Santarpia, G. W.; Crown, K. K.; Brett-Major, D. M.; Schnaubelt, E. R.; Broadhurst, M. J.; Lawler, J. V.; Reid, S. P.; Lowe, J. J. Aerosol and surface contamination of SARS-CoV-2 observed in quarantine and isolation care. *Sci. Rep.* **2020**, *10* (1), 1−8.

(7) Shiu, E. Y.; Leung, N. H.; Cowling, B. J. Controversy around airborne versus droplet transmission of respiratory viruses: implication for infection prevention. *Curr. Opin. Infect. Dis.* **2019**, *32* (4), 372−379.

(8) Somsen, G. A.; van Rijn, C.; Kooij, S.; Bem, R. A.; Bonn, D. Small droplet aerosols in poorly ventilated spaces and SARS-CoV-2 transmission. *Lancet Respir. Med.* **2020**, *8* (7), 658−659.

(9) Leung, N. H. L.; Chu, D. K. W.; Shiu, E. Y. C.; Chan, K.-H.; McDevitt, J. J.; Hau, B. J. P.; Yen, H.-L.; Li, Y.; Ip, D. K. M.; Peiris, J. S. M.; Seto, W.-H.; Leung, G. M.; Milton, D. K.; Cowling, B. J. Respiratory virus shedding in exhaled breath and efficacy of face masks. *Nat. Med.* **2020**, *26* (5), 676−680.

(10) Li, L.; Niu, M.; Zhu, Y. Assessing the effectiveness of using various face coverings to mitigate the transport of airborne particles produced by coughing indoors. *Aerosol Sci. Technol.* **2021**, *55* (3), 332−339.

(11) Dehbandi, R.; Zazouli, M. A. Stability of SARS-CoV-2 in different environmental conditions. *Lancet Microbe* **2020**, *1* (4), e145.

(12) Kariwa, H.; Fujii, N.; Takashima, I. Inactivation of SARS coronavirus by means of povidone-iodine, physical conditions, and chemical reagents. *Japanese Journal of Veterinary Research* **2004**, *52* (3), 105−112.

(13) Darnell, M. E.; Taylor, D. R. Evaluation of inactivation methods for severe acute respiratory syndrome coronavirus in noncellular blood products. *Transfusion* **2006**, *46* (10), 1770−1777.

(14) Zhong, H.; Zhu, Z.; Lin, J.; Cheung, C. F.; Lu, V. L.; Yan, F.; Chan, C.-Y.; Li, G. Reusable and recyclable graphene masks with outstanding superhydrophobic and photothermal performances. *ACS Nano* **2020**, *14* (5), 6213−6221.

(15) Kumar, S.; Karmacharya, M.; Joshi, S. R.; Gulenko, O.; Park, J.; Kim, G.-H.; Cho, Y.-K. Photoactive Antiviral Face Mask with Self-Sterilization and Reusability. *Nano Lett.* **2021**, *21* (1), 337−343.

(16) Bandaru, S.; Augustine, A.; Lepcha, A.; Sebastian, S.; Gowri, M.; Philip, A.; Mammen, M. The effects of N95 mask and face shield on speech perception among healthcare workers in the coronavirus disease 2019 pandemic scenario. *J. Laryngol. Otol.* **2020**, *134* (10), 895−898.

(17) Marler, H.; Ditton, A. I'm smiling back at you": Exploring the impact of mask wearing on communication in healthcare. *International journal of language & communication disorders* **2021**, *56* (1), 205−214.

(18) Jones, A. C.; Gutierrez, R.; Ludlow, A. K. The role of motion and intensity in deaf children's recognition of real human facial expressions of emotion. *Cognition and Emotion* **2018**, *32* (1), 102−115.

(19) Liu, C.; Hsu, P.-C.; Lee, H.-W.; Ye, M.; Zheng, G.; Liu, N.; Li, W.; Cui, Y. J. N. c. Transparent air filter for high-efficiency PM 2.5 capture. *Nat. Commun.* **2015**, *6* (1), 1−9.

(20) Khalid, B.; Bai, X.; Wei, H.; Huang, Y.; Wu, H.; Cui, Y. J. N. l. Direct blow-spinning of nanofibers on a window screen for highly efficient PM2. 5 removal. *Nano Lett.* **2017**, *17* (2), 1140−1148.

(21) Zuo, F.; Zhang, S.; Liu, H.; Fong, H.; Yin, X.; Yu, J.; Ding, B. J. S. Free-standing polyurethane nanofiber/nets air filters for effective PM capture. *Small* **2017**, *13* (46), 1702139.

(22) Heo, K. J.; Jeong, S. B.; Shin, J.; Hwang, G. B.; Ko, H. S.; Kim, Y.; Choi, D. Y.; Jung, J. H. Water-Repellent TiO2-Organic Dye-Based Air Filters for Efficient Visible-Light-Activated Photochemical Inactivation against Bioaerosols. *Nano Lett.* **2021**, *21* (4), 1576−1583.

(23) Li, P.; Li, J.; Feng, X.; Li, J.; Hao, Y.; Zhang, J.; Wang, H.; Yin, A.; Zhou, J.; Ma, X.; Wang, B. Metal-organic frameworks with photocatalytic bactericidal activity for integrated air cleaning. *Nat. Commun.* **2019**, *10* (1), 1−10.

(24) Kumar, A.; Sharma, A.; Chen, Y.; Jones, M. M.; Vanyo, S. T.; Li, C.; Visser, M. B.; Mahajan, S. D.; Sharma, R. K.; Swihart, M. T. Copper@ ZIF-8 Core-Shell Nanowires for Reusable Antimicrobial Face Masks. *Adv. Funct. Mater.* **2021**, *31* (10), 2008054.

(25) Ermini, M. L.; Voliani, V. Antimicrobial Nano-Agents: The Copper Age. *ACS Nano* **2021**, *15* (4), 6008−6029.

(26) Raha, S.; Mallick, R.; Basak, S.; Duttaroy, A. K. Is copper beneficial for COVID-19 patients? *Med. Hypotheses* **2020**, *142*, 109814.

(27) van Doremalen, N.; Bushmaker, T.; Morris, D. H.; Holbrook, M. G.; Gamble, A.; Williamson, B. N.; Tamin, A.; Harcourt, J. L.; Thornburg, N. J.; Gerber, S. I.; Lloyd-Smith, J. O.; de Wit, E.; Munster, V. J. Aerosol and surface stability of SARS-CoV-2 as compared with SARS-CoV-1. *N. Engl. J. Med.* **2020**, *382* (16), 1564−1567.

(28) Kim, D.; Kwon, J.; Jung, J.; Kim, K.; Lee, H.; Yeo, J.; Hong, S.; Han, S.; Ko, S. H. A Transparent and Flexible Capacitive-Force Touch Pad from High-Aspect-Ratio Copper Nanowires with Enhanced Oxidation Resistance for Applications in Wearable Electronics. *Small Methods* **2018**, *2* (7), 1800077.

(29) Han, S.; Hong, S.; Ham, J.; Yeo, J.; Lee, J.; Kang, B.; Lee, P.; Kwon, J.; Lee, S. S.; Yang, M.-Y.; Ko, S. H. Fast plasmonic laser nanowelding for a Cu-nanowire percolation network for flexible transparent conductors and stretchable electronics. *Adv. Mater.* **2014**, *26* (33), 5808−5814.

(30) Kratzke, I. M.; Rosenbaum, M. E.; Cox, C.; Ollila, D. W.; Kapadia, M. R. Effect of Clear vs Standard Covered Masks on Communication With Patients During Surgical Clinic Encounters: A Randomized Clinical Trial. *JAMA Surgery* **2021**, *156* (4), 372−378.

(31) Corey, R. M.; Jones, U.; Singer, A. C. Acoustic effects of medical, cloth, and transparent face masks on speech signals. *J. Acoust. Soc. Am.* **2020**, *148* (4), 2371−2375.

(32) Hori, K.; Matsumoto, S. Bacterial adhesion: from mechanism to control. *Biochem. Eng. J.* **2010**, *48* (3), 424−434.

(33) Banerjee, I.; Pangule, R. C.; Kane, R. S. Antifouling coatings: recent developments in the design of surfaces that prevent fouling by proteins, bacteria, and marine organisms. *Adv. Mater.* **2011**, *23* (6), 690−718.

(34) Chen, D.; Kang, Z.; Li, W. One-step electrodeposition to fabricate superhydrophobic coating and its reversible wettability transformation. *Mater. Res. Express* **2020**, *7* (1), 016404.

(35) Hinds, W. C. *Aerosol technology: properties, behavior, and measurement of airborne particles*, 2nd ed.; John Wiley & Sons: New York, 1999.

(36) Wang, C.-s.; Otani, Y. Removal of nanoparticles from gas streams by fibrous filters: a review. *Ind. Eng. Chem. Res.* **2013**, *52* (1), 5−17.

(37) Ge, Z.-y.; Yang, L.-m.; Xia, J.-j.; Fu, X.-h.; Zhang, Y.-z. Possible aerosol transmission of COVID-19 and special precautions in dentistry. *J. Zhejiang Univ., Sci., B* **2020**, *21* (5), 361−368.

(38) Liu, Z.-K.; Wang, Y.; Shang, S.-L. Origin of negative thermal expansion phenomenon in solids. *Scr. Mater.* **2011**, *65* (8), 664−667.

https://doi.org/10.1021/acs.nanolett.1c02737
Nano Lett. XXXX, XXX, XXX−XXX

(39) Yoon, D.; Son, Y.-W.; Cheong, H. Negative Thermal Expansion Coefficient of Graphene Measured by Raman Spectroscopy. *Nano Lett.* **2011**, *11* (8), 3227−3231.
(40) Ng, E.; Chua, L. Comparison of one-and two-dimensional programmes for predicting the state of skin burns. *Burns* **2002**, *28* (1), 27−34.
(41) Jiang, S.; Ma, N.; Li, H.; Zhang, X. Effects of thermal properties and geometrical dimensions on skin burn injuries. *Burns* **2002**, *28* (8), 713−717.
(42) Xu, F.; Lu, T.; Seffen, K.; Ng, E. Mathematical modeling of skin bioheat transfer. *Appl. Mech. Rev.* **2009**, *62* (5). DOI: 10.1115/1.3124646
(43) Ye, H.; De, S. Thermal injury of skin and subcutaneous tissues: A review of experimental approaches and numerical models. *Burns* **2017**, *43* (5), 909−932.
(44) Dupont, C. L.; Grass, G.; Rensing, C. Copper toxicity and the origin of bacterial resistance—new insights and applications†. *Metallomics* **2011**, *3* (11), 1109−1118.
(45) Jose, M.; Szymańska, K.; Szymański, K.; Moszyński, D.; Mozia, S. Effect of copper salts on the characteristics and antibacterial activity of Cu-modified titanate nanotubes. *J. Environ. Chem. Eng.* **2020**, *8* (6), 104550.
(46) Rutala, W. A.; Weber, D. J. Disinfection and sterilization: An overview. *Am. J. Infect. Control* **2013**, *41* (5), S2−S5.
(47) *Russell, Hugo and Ayliffe's principles and practice of disinfection, preservation & sterilization*, 6th ed.; Fraise, A. P., Lambert, P. A., Masillard, J.-Y., Eds.; Blackwell Publishing: Cambridge, 2004.
(48) Yoon, K.-Y.; Hoon Byeon, J.; Park, J.-H.; Hwang, J. Susceptibility constants of Escherichia coli and Bacillus subtilis to silver and copper nanoparticles. *Sci. Total Environ.* **2007**, *373* (2), 572−575.
(49) Kim, J.-H.; Ma, J.; Jo, S.; Lee, S.; Kim, C. S. Enhancement of Antibacterial Properties of a Silver Nanowire Film via Electron Beam Irradiation. *ACS Applied Bio Materials* **2020**, *3* (4), 2117−2124.
(50) Sun, D.; Wang, A.; Cheng, S.; Yates, M.; Logan, B. E. Geobacter anodireducens sp. nov., an exoelectrogenic microbe in bioelectrochemical systems. *Int. J. Syst. Evol. Microbiol.* **2014**, *64* (Pt_10), 3485−3491.
(51) Yamashita, T.; Ishida, M.; Asakawa, S.; Kanamori, H.; Sasaki, H.; Ogino, A.; Katayose, Y.; Hatta, T.; Yokoyama, H. Enhanced electrical power generation using flame-oxidized stainless steel anode in microbial fuel cells and the anodic community structure. *Biotechnol. Biofuels* **2016**, *9* (1), 62.
(52) Beuth, L.; Pfeiffer, C. P.; Schröder, U. Copper-bottomed: electrochemically active bacteria exploit conductive sulphide networks for enhanced electrogeneity. *Energy Environ. Sci.* **2020**, *13* (9), 3102−3109.
(53) Allison, A. L.; Ambrose-Dempster, E.; Domenech Aparsi, T.; et al. The environmental dangers of employing single-use face masks as part of a COVID-19 exit strategy. 2020, *UCL Open: Environment Preprint.* DOI: DOI: 10.14324/111.444/000031.v1 (accessed May 11, 2021).
(54) Jeong, S.; Cho, H.; Han, S.; Won, P.; Lee, H.; Hong, S.; Yeo, J.; Kwon, J.; Ko, S. H. High Efficiency, Transparent, Reusable, and Active PM2.5 Filters by Hierarchical Ag Nanowire Percolation Network. *Nano Lett.* **2017**, *17* (7), 4339−4346.
(55) Zhang, G.-H.; Zhu, Q.-H.; Zhang, L.; Yong, F.; Zhang, Z.; Wang, S.-L.; Wang, Y.; He, L.; Tao, G.-H. High-performance particulate matter including nanoscale particle removal by a self-powered air filter. *Nat. Commun.* **2020**, *11* (1), 1653.
(56) Ji, Z.; Dai, R.; Zhang, Z. Characterization of fine particulate matter in ambient air by combining TEM and multiple spectroscopic techniques − NMR, FTIR and Raman spectroscopy. *Environmental Science: Processes & Impacts* **2015**, *17* (3), 552−560.
(57) Polidori, A.; Turpin, B. J.; Davidson, C. I.; Rodenburg, L. A.; Maimone, F. Organic PM2.5: Fractionation by Polarity, FTIR Spectroscopy, and OM/OC Ratio for the Pittsburgh Aerosol. *Aerosol Sci. Technol.* **2008**, *42* (3), 233−246.

https://doi.org/10.1021/acs.nanolett.1c02737
Nano Lett. XXXX, XXX, XXX−XXX